Thermal independent Silicon-Nitride slot waveguide biosensor with high sensitivity

Xiaoguang Tu,[1,*] Junfeng Song,[1,2] Tsung-Yang Liow,[1] Mi Kyoung Park,[1] Jessie Quah Yiying,[1] Jack Sheng Kee,[1] Mingbin Yu,[1] and Guo-Qiang Lo[1]

[1]*Institute of Microelectronics, A*STAR (Agency for Science, Technology and Research), 11 Science Park Road, Singapore Science Park II, 117685, Singapore*

[2]*State Key Laboratory on Integrated opto-electronics, College of Electronic Science and Engineering, Jilin University, Changchun, 130023 China*

[*]*tux@ime.a-star.edu.sg*

Abstract: As the sensitivity and detection limit of photonic refractive index (RI) biosensor increases, the temperature dependence becomes a major challenge. In this paper, we present a Mach-Zehnder Interferometer (MZI) biosensor based on silicon nitride slot waveguides. The biosensor is designed for minimal temperature dependence without compromising the performance in terms of sensitivity and detection limit. With air cladding, the measured surface sensitivity and detection limit of MZI biosensor reach 7.16 nm/ (ngmm^{-2}) and 1.30 (pgmm^{-2}), while achieving a low temperature dependence is 5.0 pm/^{o} C. With water cladding, the measured bulk sensitivity and detection limit reach 1730(2π)/RIU and 1.29 × 10^{-5} RIU respectively. By utilizing Vernier effect through cascaded MZI structures, the measured sensitivity enhancement factor is 8.38, which results in a surface detection limit of 0.155 (pgmm^{-2}).

OCIS codes: (130.3120) Integrated optics devices; (230.7370) Waveguides; (130.6010) Sensors; (230.3990) Microstructure devices.

References and links

1. X. D. Fan, I. M. White, S. I. Shopova, H. Y. Zhu, J. D. Suter, and Y. Z. Sun, "Sensitive optical biosensors for unlabeled targets: a review," Anal. Chim. Acta **620**(1-2), 8–26 (2008).
2. R. Narayanaswamy and O. S. Wolfbeis, *Optical Sensors*, (Springer, 2004).
3. B. Liedberg, C. Nylander, and I. Lundstrom, "Biosensing with surface Plasmon resonance-how it all started," Biosens. Bioelectron. **10**(8), i–ix (1995).
4. J. Melendez, R. Carr, D. U. Bartholomew, K. Kukanskis, J. Elkind, S. Yee, C. Furlong, and R. Woodbury, "A commercial solution for surface Plasmon sensing," Sens. Actuators B Chem. **35**(1-3), 212–216 (1996).
5. C. Y. Chao and L. J. Guo, "Biochemical sensors based on polymer microrings with sharp asymmetrical resonance," Appl. Phys. Lett. **83**(8), 1527–1529 (2003).
6. M. Iqbal, M. A. Gleeson, B. Spaugh, F. Tybor, W. G. Gunn, M. Hochberg, T. B. Jones, R. C. Bailey, and L. C. Gunn, "Laber-Free biosensor arrays based on silicon ring resonators and high-speed optical scanning instrumentation," IEEE J. Sel. Top. Quantum Electron. **16**(3), 654–661 (2010).
7. D. X. Dai, "Highly sensitive digital optical sensor based on cascaded high-Q ring-resonators," Opt. Express **17**(26), 23817–23822 (2009).
8. T. Claes, W. Bogaerts, and P. Bienstman, "Experimental characterization of a silicon photonic biosensor consisting of two cascaded ring resonators based on the Vernier-effect and introduction of a curve fitting method for an improved detection limit," Opt. Express **18**(22), 22747–22761 (2010).
9. L. Jin, M. Y. Li, and J. J. He, "Optical waveguide double-ring sensor using intensity interrogation with a low-cost broadband source," Opt. Lett. **36**(7), 1128–1130 (2011).
10. C. A. Barrios, K. B. Gylfason, B. Sánchez, A. Griol, H. Sohlström, M. Holgado, and R. Casquel, "Slot-waveguide biochemical sensor," Opt. Lett. **32**(21), 3080–3082 (2007).
11. C. F. Carlborg, K. B. Gylfason, A. Kaźmierczak, F. Dortu, M. J. Bañuls Polo, A. Maquieira Catala, G. M. Kresbach, H. Sohlström, T. Moh, L. Vivien, J. Popplewell, G. Ronan, C. A. Barrios, G. Stemme, and W. van der Wijngaart, "A packaged optical slot-waveguide ring resonator sensor array for multiplex label-free assays in labs-on-chips," Lab Chip **10**(3), 281–290 (2010).
12. A. Densmore, M. Vachon, D. X. Xu, S. Janz, R. Ma, Y. H. Li, G. Lopinski, A. Delâge, J. Lapointe, C. C. Luebbert, Q. Y. Liu, P. Cheben, and J. H. Schmid, "Silicon photonic wire biosensor array for multiplexed real-time and label-free molecular detection," Opt. Lett. **34**(23), 3598–3600 (2009).

#157062 - $15.00 USD Received 25 Oct 2011; revised 8 Dec 2011; accepted 13 Dec 2011; published 20 Jan 2012

13. D. X. Xu, M. Vachon, A. Densmore, R. Ma, S. Janz, A. Delâge, J. Lapointe, P. Cheben, J. H. Schmid, E. Post, S. Messaoudène, and J. M. Fédéli, "Real-time cancellation of temperature induced resonance shifts in SOI wire waveguide ring resonator label-free biosensor arrays," Opt. Express **18**(22), 22867–22879 (2010).
14. K. B. Gylfason, C. F. Carlborg, A. Kaźmierczak, F. Dortu, H. Sohlström, L. Vivien, C. A. Barrios, W. van der Wijngaart, and G. Stemme, "On-chip temperature compensation in an integrated slot-waveguide ring resonator refractive index sensor array," Opt. Express **18**(4), 3226–3237 (2010).
15. J. Teng, P. Dumon, W. Bogaerts, H. B. Zhang, X Jian, X Han, M. S. Zhao, G. Morthier, and R. Baets, "Athermal Silicon-on-insulator ring resonators by overlaying a polymer cladding on narrowed waveguides," Opt. Express **17**(17), 14627–14633 (2009).
16. M. Uenuma and T. Moooka, "Temperature-independent silicon waveguide optical filter," Opt. Lett. **34**(5), 599–601 (2009).
17. B. Guha, A. Gondarenko, and M. Lipson, "Minimizing temperature sensitivity of silicon Mach-Zehnder interferometers," Opt. Express **18**(3), 1879–1887 (2010).
18. B. Guha, B. B. C. Kyotoku, and M. Lipson, "CMOS-compatible athermal silicon microring resonators," Opt. Express **18**(4), 3487–3493 (2010).
19. R. Amatya, C. W. Holzwarth, H. I. Smith and R. J. Ram, "Efficient thermal tuning for second-order silicon nitride microring resonators," Photonics. In. Switching, 149–150 (2007).
20. C. B. Kim and C. B. Su, "Measurement of the refractive index of liquids at 1.3 and 1.5 micron using a fibre optic Fresnel ratio meter," Meas. Sci. Technol. **15**(9), 1683–1686 (2004).
21. H. Su and X. G. Huang, "Fresnel-reflection-based fiber sensor for on-line measurement of solute concentration in solutions," Sens. Actuators B Chem. **126**(2), 579–582 (2007).
22. I. M. White and X. D. Fan, "On the performance quantification of resonant refractive index sensors," Opt. Express **16**(2), 1020–1028 (2008).
23. D.-X. Xu, M. Vachon, A. Densmore, R. Ma, A. Delâge, S. Janz, J. Lapointe, Y. Li, G. Lopinski, D. Zhang, Q. Y. Liu, P. Cheben, and J. H. Schmid, "Label-free biosensor array based on silicon-on-insulator ring resonators addressed using a WDM approach," Opt. Lett. **35**(16), 2771–2773 (2010).

1. Introduction

Label-free detection and fluorescence-based detection are the two main detection protocols in optical chemical biosensor. As in the label-free detection, the target molecules are not labeled and quantitative and kinetic measurement of molecular interaction is allowed, this type of detection is more preferred than fluorescence-based detection [1,2]. Refractive index (RI) change method is one of label-free detection methods, in which the change of sample concentration or surface density induces the change of RI. As only a small volume of sample is enough for detection, RI chemical biosensor attracts much attention by combing with versatile optical structures. Corresponding designs include surface plasma biosensor [3,4] and evanescent field waveguide biosensor such as the silicon-waveguide-based micro-ring resonators and array [5,6], the cascaded ring resonators (which can realize extremely high sensitivity through Vernier effect) [7–9], the silicon slot waveguide ring resonators and array [10,11] and silicon waveguide Mach-Zehnder Interferometer (MZI) [12].

Besides the improvement of the sensing sensitivity and detection limit, in order to bring the sensor from laboratory to market with actual applications, another important consideration is the signal to noise ratio. For a biosensor, one of the most important noise sources from the environment is the thermal noise. In the reported photonic RI biosensors cited earlier, the temperature is typically controlled by adding a temperature-controlled system underneath the biosensor. Such systems are complex and may only be sufficient for the low sensitivity detection. For the biosensor with very high sensitivity, thermal noise will affect the testing results significantly.

Previously, real-time cancellation of temperature influence is realized through a reference ring in order to track the temperature changes by using silicon wire and silicon nitride (SiN) slot waveguide ring-based sensor arrays [13,14]. However, both the fabrication processing and the data analysis processing are complex. Athermal performance is also demonstrated by using cladding layer with compensated thermo-optic coefficient [15]. However, it is not compatible with CMOS processes. The ideal way to realize athermal performance of biosensor would likely be passive, simple and CMOS compatible. One choice is an asymmetric MZI structure through which perfect temperature independence has been realized on silicon-on-insulator platform [16–18]. However, to the best of our knowledge, there are no reports on reducing the temperature dependence of biosensor by using this approach.

#157062 - $15.00 USD Received 25 Oct 2011; revised 8 Dec 2011; accepted 13 Dec 2011; published 20 Jan 2012

In this paper, by combining the athermal optical filter with SiN slot waveguide, we present an optical biosensor which can realize temperature independence without compromising on the high sensitivity performance. Moreover, we demonstrate a thermal independent biosensor with higher sensitivity through cascaded MZIs by utilizing the Vernier effect.

2. Design and principles

From a structural perspective, slot waveguide has an intrinsic merit for confining light into a nanometer-size slot. Thereafter, once a cladding material is filled into this small slot, it will result in a strong interaction between the incident light and the cladding material. This special mechanism makes slot waveguide an ideal candidate for the application of high sensitivity biosensors. From a material perspective, SiN has a much lower thermal-optic coefficient than silicon which makes it a good choice for athermal photonic devices design. Figure 1 illustrates the structure of SiN slot waveguide MZI biosensors. In Fig. 1, a sensing window is opened on the surface of the MZI for the biochemical target. In the MZI biosensor, the reference arm is composed by SiN strip waveguide with length of L and SiN connecting waveguide. The sensing arm is composed by a SiN slot waveguide with length of L, two SiN strip waveguides with length of $\Delta L/2$ and also a SiN connecting waveguide. The cross-section of SiN strip waveguide and SiN slot waveguide are denoted by a-a' and b-b' respectively. The connecting waveguides have an identical length between sensing arm and reference arm. The width of SiN strip waveguide and slot waveguide are denoted as w_s, w_h and w_l respectively. The slab heights of both strip and slot waveguide are t_s. There is a silicon oxide cladding layer on the surface of the SiN strip waveguide with thickness of t_c. This cladding layer separates the influence of sensing target from the strip waveguide and leaves the slot waveguide the only active sensing part of the MZI biosensor.

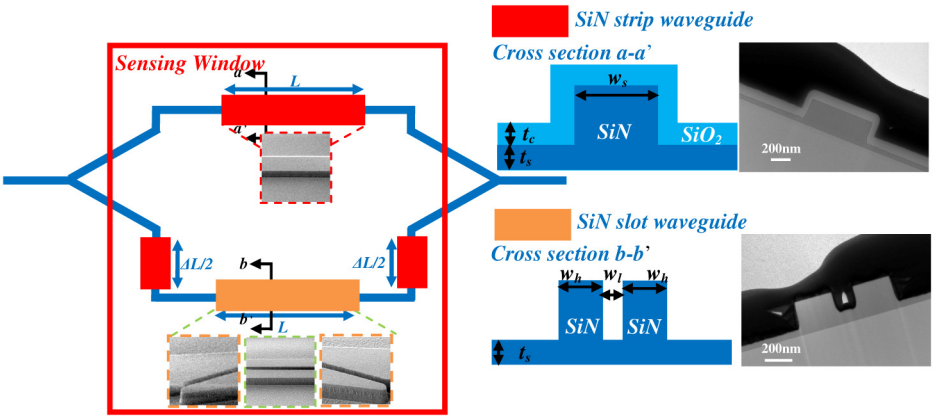

Fig. 1. Plan-view and cross-section schematics of the athermal MZI biosensor. Cross sections schematics and TEM images of different arms are also shown.

Following the MZI theory, the output of MZI biosensor can be expressed as:

$$\frac{I_{out}}{I_{in}} = \frac{1}{2}(1+\cos\phi), \phi = \frac{2\pi}{\lambda}[(n_{eff\_slot} - n_{eff\_strip})L + n_{eff\_strip}\Delta L], \quad (1)$$

where n_{eff_slot} and n_{eff_strip} denote the effective refractive index of SiN slot and strip waveguide while φ is the phase difference between two arms.

When the refractive index of the biochemical changes is Δn_{eff_slot}, the corresponding phase shift $\Delta\varphi$ and wavelength shift $\Delta\lambda$ satisfy:

$$\Delta\phi = \frac{2\pi}{\lambda}\Delta n_{eff\_slot} \cdot L, \quad (2)$$

#157062 - $15.00 USD Received 25 Oct 2011; revised 8 Dec 2011; accepted 13 Dec 2011; published 20 Jan 2012

$$\frac{\Delta\lambda}{\lambda} = \frac{\Delta n_{eff\_slot} \cdot L}{(n_{g\_slot} - n_{g\_strip})L + n_{g\_strip}\Delta L}, \tag{3}$$

where n_{g_slot} and n_{g_strip} are the group indices of the slot and strip waveguide, respectively. The free spectral range (FSR_s) of the MZI biosensor is:

$$FSR_s(\lambda) = \frac{\lambda}{M} = \frac{\lambda^2}{(n_{g\_slot} - n_{g\_strip})L + n_{g\_strip}\Delta L}, \tag{4}$$

in which M denotes the interference order under wavelength λ considering the wavelength dispersion [16]. Considering the thermo-optic effect of the device, the temperature dependence of the output spectrum is:

$$\frac{\partial\lambda}{\partial T} = \frac{\Delta L}{M}\frac{\partial n_{neff\_strip}}{\partial T} + \frac{L}{M}\frac{\partial(n_{neff\_slot} - n_{neff\_strip})}{\partial T}, \tag{5}$$

It should be noted that thermal expansion effect of SiN waveguide also contributes to the wavelength shift of the structure. However, compared to that of thermo-optic effect, this kind of influence is much smaller and can be neglected. From Eq. (5), temperature independence can be achieved by making the right side of equation equal to zero, which means the thermo-optic coefficient satisfies:

$$\frac{\partial n_{neff\_strip}}{\partial T}(L - \Delta L) = \frac{\partial n_{neff\_slot}}{\partial T}L, \tag{6}$$

3. Experimental and discussion

The biosensor was fabricated on silicon substrate with 3 μm buried oxide layer using standard CMOS processes. The widths of the strip and slot waveguide were w_s = 1 μm, w_h = 440 nm and w_l = 190 nm, respectively. The thickness of the SiN waveguide was 400nm with t_s = 80nm slab. The arm with strip SiN waveguide of the MZI was covered with t_c = 150 nm oxide cladding. The arm with slot SiN waveguide had no cladding layer. There was a pair of mode coupler between the strip and slot waveguide for low loss mode coupling. Uniform nano-tips were integrated on the input and output end of the waveguide for fiber coupling. After dicing, the chips were covered with polydimethylsiloxane (PDMS) on which micro tubes were prepared to make the micro fluid channel. The biosensor was tested under a 6 axis optical fiber-to-waveguide alignment system. The output of the MZI biosensor first went through an optical spectrum analysis (OSA) with an amplified spontaneous emission (ASE) laser source. Subsequently, a photodetector was utilized to see the phase shift changes by time with a fixed wavelength coming from a tunable laser. The temperature of the chip was adjusted and tested with a thermal electric cooler (TEC) and temperature sensor. The spectra were measured and saved with the temperature changing from 23.5° C to 42.7° C. The measured TE-mode transmission loss of SiN strip and slot waveguide was 0.602 dB/cm and 0.872 dB/cm with insertion loss of the mode coupler as low as 0.03 dB/pair. The measured results are discussed below.

3.1 Thermal dependence

According to Eq. (6), we design the cross section and length of the sensing and reference arms after detailed simulations (which will not be discussed here). The measured normalized transmission spectra at different temperatures for five values of $\Delta L/L$ are shown in Fig. 2. All spectra are normalized with a strip SiN waveguide.

#157062 - $15.00 USD Received 25 Oct 2011; revised 8 Dec 2011; accepted 13 Dec 2011; published 20 Jan 2012

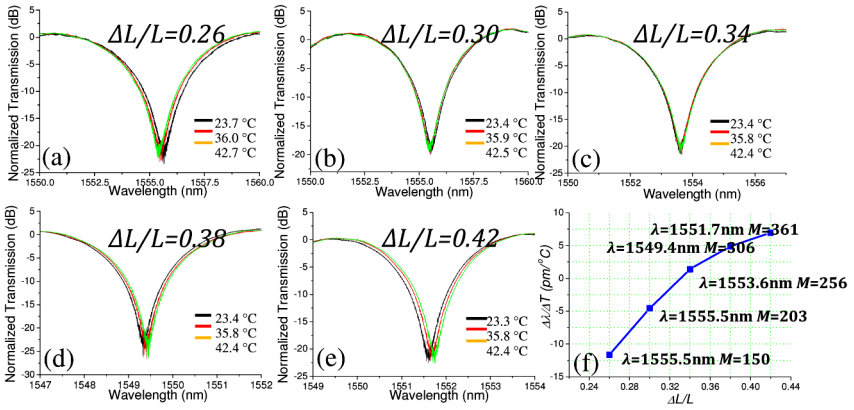

Fig. 2. The (a-e) measured transmission spectra of MZI biosensor with air cladding and (f) temperature dependence $\partial\lambda/\partial T$ under different $\Delta L/L$. Here we fix L = 1 mm as an example.

On the transmitted spectra, the temperature dependence of MZI biosensor $\partial\lambda/\partial T$ changes from negative to positive as $\Delta L/L$ changes from 0.26 to 0.42. Thermal independence is realized with $\Delta L/L$ = 0.33 which results in the thermo-optic coefficient ratio $r = (\partial n_{eff\_slot}/\partial T)/(\partial n_{eff\_strip}/\partial T) \approx 0.67$ according to Eq. (6). Within the region of $\partial\lambda/\partial T$ = (+/−5) pm/° C, $\Delta L/L$ is allowed to vary from 0.30 to 0.38. Given L = 1mm, ΔL is allowed to vary from 300μm to 380μm, which suggests an extremely large tolerance in the fabrication process. The nonlinear relationship between $\partial\lambda/\partial T$ and $\Delta L/L$ comes from the wavelength dependence of the thermo-optic coefficient of strip and slot SiN waveguide. The measured wavelength and interference order M are also denoted in Fig. 2(f). Near the temperature independent point ($\Delta L/L$ = 0.33, r~0.67), the measured thermo-optic coefficient of TE mode in strip and slot waveguide is $\partial n_{eff\_strip}/\partial T = 3.58 \times 10^{-5}$ /° C and $\partial n_{eff\_slot}/\partial T = 2.43 \times 10^{-5}$ /° C at λ = 1550nm which is compatible with that of the simulation result ($\partial n_{eff\_strip}/\partial T = 3.49 \times 10^{-5}$ /° C, and r~0.69) by using thermo-optic coefficients of oxide to be $\partial n_{oxide}/\partial T = 1.0 \times 10^{-5}$ /° C and SiN to be $\partial n_{SiN}/\partial T = 4.0 \times 10^{-5}$ /° C, respectively [19]. Because of the special athermal design and small thermo-optic coefficient of SiN compared with that of silicon ($\partial n_{silicon}/\partial T = 1.84 \times 10^{-4}$ /° C), the temperature dependence of the SiN slot waveguide MZI is much lower than that of silicon MZI. Here we choose L = 1 mm as an example. It should be noted that for a fixed $\Delta L/L$, the athermal performance of the SiN slot waveguide MZI is independent of the L. Thereafter, we can keep the low temperature dependence of the biosensor with fixed $\Delta L/L$ and increase the sensitivity of the biosensor with larger L, which will be demonstrated in the following section. It should be noted that this particular $\Delta L/L$ value is only applicable for air cladding case. For the actual biosensor, the true value of $\Delta L/L$ depends on the thermo-optic coefficient of target chemical solution, and has to be taken into account. Take water cladding as an example (the thermo-optic coefficient of water is $\partial n_{water}/\partial T = -8.0 \times 10^{-5}$ /° C [20]), the calculated athermal condition is satisfied under $\Delta L/L$ = 0.83 which is different from that of air cladding case. However, because phase shift $\Delta\varphi$ depends more on the absolute value of L instead of $\Delta L/L$ as shown in Eq. (2), different value of $\Delta L/L$ will not degrade the phase shift sensitivity of this design.

2. Bulk sensitivity

We perform time-sampled measurements on the bulk sensitivity of MZI biosensor using NaCl solution with different concentration at λ = 1542.0 nm using a tunable laser source. The output light is collected and transferred to electrical current signal through a high speed IR photodetector (PD) with a responsibility of 0.45 A/W. The output electrical signal of the PD is collected into an Agilent semiconductor device parameter analyzer. When the measurement is started, water and NaCl solution with different concentration are pumped from a reservoir into

#157062 - $15.00 USD Received 25 Oct 2011; revised 8 Dec 2011; accepted 13 Dec 2011; published 20 Jan 2012

the micro fluidic channel using a peristaltic pump. We switch back to water after the output signal is stable in order to check the reliability of the measured data. The measured results are shown in Fig. 3(a-e).

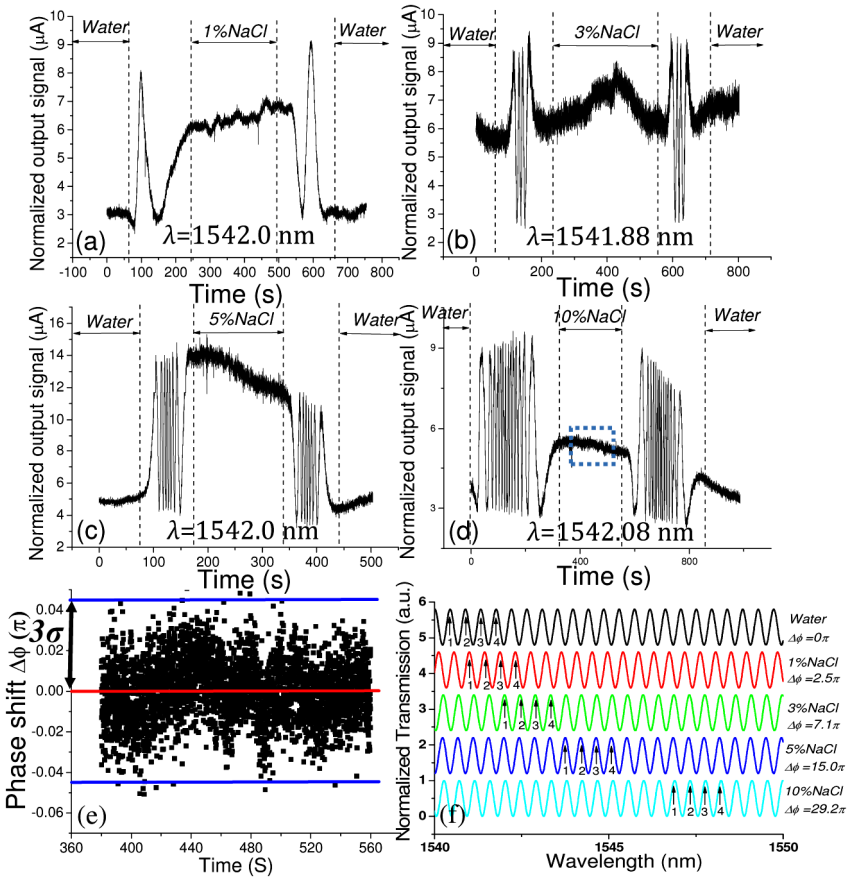

Fig. 3. Spectra of MZI biosensor with L = 7 mm and $\Delta L/L$ = 0.396 under NaCl solution with different concentration. (a-d) Measured photocurrent of the photodetector at the output of the MZI biosensor with time with (a) water-1% NaCl-water under λ = 1542.0 nm (b) water-3% NaCl-water under λ = 1541.88 nm (c) water-5% NaCl-water under λ = 1542.0 nm (d) water-10% NaCl-water under λ = 1542.08 nm. (e) zoomed-in view of Fig. 3(d) which shows standard deviation of amplitude noise σ (f) Fitted spectra and phase shift of the MZI biosensor under NaCl solution with different concentration in which No.1-4 denotes different peaks. The measured free spectral range of the sensor with water cladding is FSR_s = 0.42 nm.

When the fluid flowing in the micro-fluidic channel is switched to NaCl solution, the effective refractive index of the slot waveguide mode is increased which induces red shift of the peaks with No. 1-4 on Fig. 3(f). As a result, the output of MZI changes in a periodic fashion, which results in the corresponding oscillation of the photocurrent along with time. Larger NaCl concentration induces larger refractive index shift and higher numbers of the oscillations. As the switching process is finished, the output photocurrent stays stable. When the fluid is switched back to water, the above process is reversed and blue-shift is observed, as expected. The output photocurrent shows a reversed course and after stablization, the photocurrent is nearly the same as that at the beginning. The RI of NaCl solution with p% concentration is calculated by n (p%)=1.3105+0.17151×p% [21]. Measured bulk sensitivity of MZI biosensor with L=7 mm and $\Delta L/L$ = 0.396 is S_b=1730 (2π) /RIU as shown in Fig. 4. Following the magnification of the measured standard deviation 3σ =0.0446 π in Fig. 3(e)

#157062 - $15.00 USD Received 25 Oct 2011; revised 8 Dec 2011; accepted 13 Dec 2011; published 20 Jan 2012

[22], the bulk refractive index detection limit using 3 standard deviations is $DL_b=3\sigma/S_b$=1.29 ×10^{-5} *RIU*.

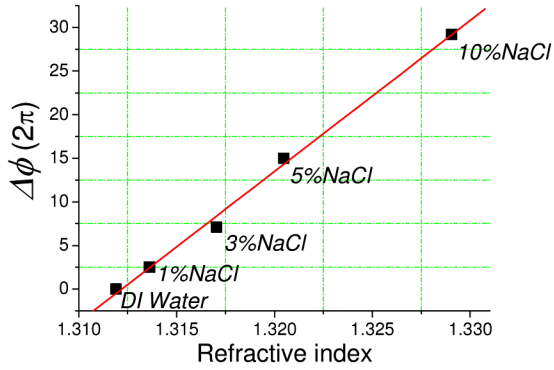

Fig. 4. The measured phase shift (2π) of MZI biosensor with L=7 mm and $\Delta L/L$=0.396 according to the refractive index of chemical target. The measured bulk sensitivity reaches 1730 (2π)/RIU with detection limit of 1.29×10^{-5} RIU.

3.3 Surface sensitivity

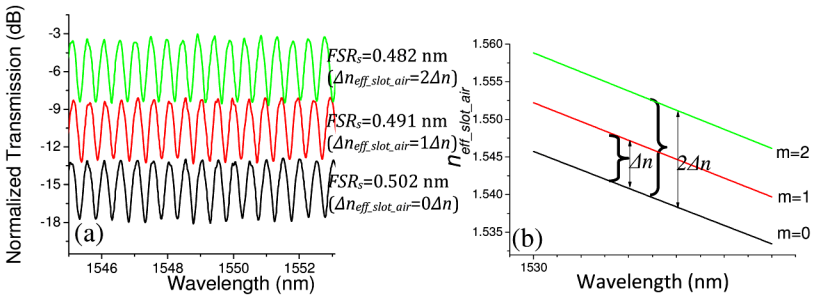

Fig. 5. The measured transmission (a) spectra and (b) effective RI shift of slot waveguide with air cladding $\Delta n_{eff\_slot\_air}$ under different bilayer of cladding polymer with L = 7 mm and $\Delta L/L$ = 0.396 mm. Δn denotes the unit of changes of $n_{eff\_slot\_air}$ according to the relationship $\Delta n_{eff\_slot\_air}$ = $m\,\Delta n$ in which m denotes the number of bilayer.

Surface sensitivity measurement is conducted by testing the transmission spectra after cladding the surface of the devices with different number of bilayers. The number of each bilayer is denoted as m. Before polymer cladding, the device is firstly immersed in a solution of 2% 3-aminopropyltriethoxysilane (APTES) in a mixture of ethanol/H_2O (95%/5%) for 2 hrs to give a positively charged surface. After that, the device is thoroughly rinsed with ethanol and DI water. Polyelectrolyte multilayer film is built by alternately immersing the device in aqueous solutions of poly (sodium-4-styrenesulfonate) (PSS, 1 mg/mL in 50 mM NaCl) and poly (allylamine hydrochloride) (PAH, 1 mg/mL in 50 mM NaCl) for 15 min each. After each polymer deposition, the device is rinsed three times in DI water followed by nitrogen drying. By repeating PSS and PAH deposition, a desired thickness of the polymer layer on the device can be obtained. The thickness of each bilayer (PSS/PAH) is 2 nm, with a surface density ~2.0 (ngmm^{-2}). The measured spectra and surface sensitivity of MZI biosensor are shown in Fig. 5. We fit the transmission spectra and FSR_s under different number of bilayers by considering the waveguide mode dispersion. The measured Δn at 1550nm reaches 6.46 × 10^{-3} and $\Delta\lambda$ = 14.33 nm following Eq. (3). The group indices of strip and slot waveguide at λ = 1550nm are n_{g_strip} = 2.0534 and n_{g_slot} = 1.9218 respectively. With sensor resolution 3σ = 9.33 pm, the surface sensitivity and detection limit are S_s = $\Delta\lambda$/2.0 (ngmm^{-2}) = 7.16 nm/ (ngmm^{-2}) and DL_s = 3 σ /S_s = 1.30 (pgmm^{-2}) as shown in Table 1.

#157062 - $15.00 USD Received 25 Oct 2011; revised 8 Dec 2011; accepted 13 Dec 2011; published 20 Jan 2012

Table 1. Measured surface sensitivity of one and two MZI biosensor.

Layer no	m=0	m=1	m=2	m=3	m=4	Δn @1550nm	$\Delta\lambda$ (nm)	Surface Sensitivity	Detection limit
One MZI	FSR_s (nm)					6.46e-3	14.33	7.16 nm/ (ngmm^{-2})	1.30 pgmm^{-2}
	0.502	0.491	0.482	0.476	0.469				
Cascaded MZI	FSR_r (nm)						120.07 (K = 8.38)	60.00 nm/ (ngmm^{-2}) (K = 8.38)	0.155 pgmm^{-2} (K = 8.38)
	0.571	0.568	0.569	0.570	0.570				
	FSR_c (nm)								
	4.14	3.63	3.15	2.88	2.64				

3.4 Surface sensitivity of cascaded MZI

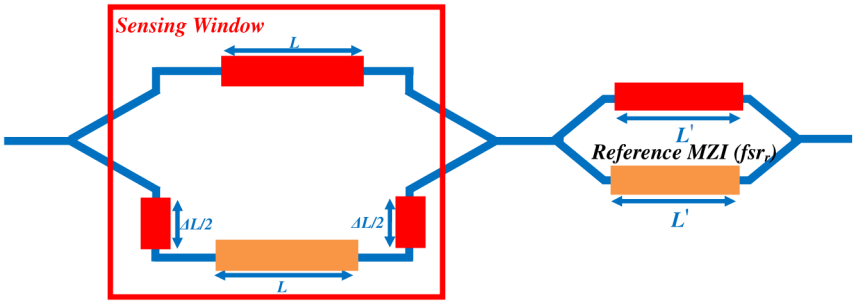

Fig. 6. Schematic of cascaded athermal MZI biosensor with L = 7 mm, $\Delta L/L$ = 0.396 and L' = 26.1 mm. In the cascaded MZI biosensor, the reference MZI is covered with 2 μm-thick oxide cladding layer. The Free Spectrum Range of sensing MZI, reference MZI and cascaded MZI are denoted as FSR_s, FSR_r and FSR_c respectively.

A cascaded MZI biosensor is formed by cascading a reference MZI after the sensing MZI as shown in Fig. 6. The reference MZI is covered with a 2 μm-thick oxide cladding layer. Compared to a conventional MZI biosensor, the sensitivity of cascaded MZI biosensor will be increased through the Vernier effect. The enhancement factor K depends on the free spectral range of the sensing MZI FSR_s and reference MZI FSR_r. Vernier effect is widely utilized to enhance the measurement accuracy which can also be used to enhance the sensitivity of biosensor. According to Vernier effect, the FSR of the overlap of the output spectrum FSR_c and the sensitivity enhancement factor K can be expressed as:

$$FSR_c = \frac{FSR_s \cdot FSR_r}{|FSR_s - FSR_r|}, K = \frac{FSR_r}{|FSR_s - FSR_r|} \tag{7}$$

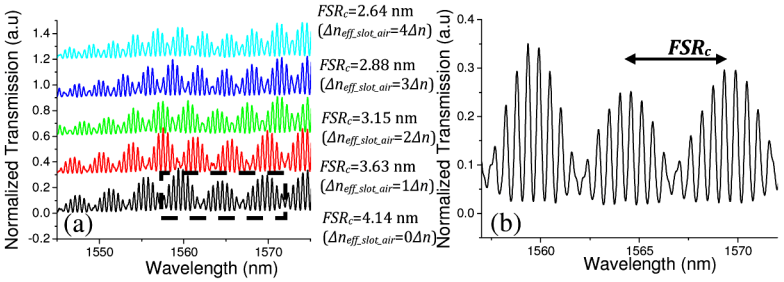

Fig. 7. The output spectra of cascaded MZI biosensor (a) under different bilayers of PSS/PAH and (b) Zoomed-in view of (a) with m=0.

The key to enhance the sensitivity through the Vernier effect is to reduce the different between FSR_r and FSR_s. In Fig. 7, the measured FSR of sensing MZI and reference MZI with water solution are FSR_s=0.502 nm and FSR_r=0.570 nm respectively, corresponding to an enhancement factor of K=8.38. With this enhancement factor, the surface sensitivity and

#157062 - $15.00 USD Received 25 Oct 2011; revised 8 Dec 2011; accepted 13 Dec 2011; published 20 Jan 2012

detection limit of the cascaded MZI biosensor reach 60.00 nm/ ($ngmm^{-2}$) and 0.155 ($pgmm^{-2}$) as shown in Table 1. As far as we know, this result is comparable with the best report result which is 0.3 ($pgmm^{-2}$) [23]. Moreover, by integrating with the athermal structure, our device achieves lower temperature dependence at the same time.

4. Conclusion

The temperature dependence of the photonic biosensor is greatly reduced by using low loss silicon nitride slot waveguide MZI system. For the MZI biosensor with air cladding, temperature dependence of 5 pm /^{o} C is realized with a surface sensitivity as high as 7.16nm/ ($ngmm^{-2}$). By cascading two MZI together, even higher detection limit 0.155 ($pgmm^{-2}$) can be realized. When the biosensor is used for chemical target with different thermo-optic coefficient, athermal performance can be realized by adjusting the waveguide length ratio accordingly. Due to the lower waveguide loss and thermo-optic dependence in SiN material compared with that of silicon, SiN slot waveguide shows much better performance than silicon waveguide especially in the application of athermal biosensors. Furthermore, this design shows a large fabrication tolerance which reduces the difficulty for manufacturing and actual usage.

#157062 - $15.00 USD Received 25 Oct 2011; revised 8 Dec 2011; accepted 13 Dec 2011; published 20 Jan 2012